The effect of ionic group rotations on proton orderings in $M_3H(XO_4)_2$ super-ionic crystals

1998 J. Phys.: Condens. Matter 10 7079

(http://iopscience.iop.org/0953-8984/10/31/023)

J. Phys.: Condens. Matter **10** (1998) 7079–7090. Printed in the UK PII: S0953-8984(98)92541-3

The effect of ionic group rotations on proton orderings in $M_3H(XO_4)_2$ super-ionic crystals

I V Stasyuk† and N Pavlenko‡

Institute for Condensed Matter Physics of the National Academy of Sciences of Ukraine, 1 Svientsitsky Street, UA-290011 Lviv, Ukraine

Received 16 March 1998

Abstract. The various proton orderings occurring in $M_3H(XO_4)_2$ crystals are investigated in the framework of a lattice-gas-type model with account taken of the interactions of the proton subsystem with the orientations of the XO_4 ionic groups. In particular, it is shown that the orientational ordering of SeO_4 ions is strongly involved in the I–II–III–IV phase transitions which take place in $(NH_4)_3H(SeO_4)_2$ and appears to be the basic mechanism determining the observed phase sequence. The phase diagram obtained together with the microscopic parameter values calculated for $(NH_4)_3H(SeO_4)_2$ agree with the experimental data for the phase orderings.

1. Introduction

The $M_3H(XO_4)_2$ (M = K, Rb, Cs, NH_4; X = Se, S) family of crystals has attracted much attention—at first in view of their ferroelectric properties, and lately owing to the discovery of the high-temperature super-ionic phases with protonic conductivity. In these compounds, with layered structure, the XO_4 tetrahedra together with protons form the conducting planes of the virtual hydrogen bonds. The conduction mechanism is complicated due to the interplay of the vertex oxygens O(2) of the disordered XO_4 groups and protons on the hydrogen bridges, and consists in the dynamical formation and breaking of the hydrogen bonds between the O(2) oxygens with a one-third probability of each hydrogen bond existing.

It is worthy of note that the super-ionic phase transitions in these crystals are of ferroelastic nature also. The ordered sequences of the dimers consisting of XO_4 tetrahedra connected by the hydrogen bonds O(2)′–H–O(2)″ arise in the low-temperature ferroelastic phases of monoclinic or even triclinic symmetry. The crystals which belong to this family are isomorphic and that is the reason for the similarity of the phase sequences occurring in them. In most cases the super-ionic phase of trigonal symmetry $R\bar{3}m$ transforms on cooling into the ferroelastic phase of monoclinic symmetry $C2/c$ (or $A2/a$) with the further ferroelectric ordering that is observed in $Rb_3H(SeO_4)_2$ and $Cs_3H(SeO_4)_2$ crystals for example [1–4]. According to recent structural studies [5–7] a more complicated phase sequence occurs in $(NH_4)_3H(SeO_4)_2$ (TAHSe) crystal: phase I (trigonal $R\bar{3}m$), phase II (trigonal $R\bar{3}$), phase III (triclinic $C\bar{1}$), phase IV (monoclinic $C2/c$), phase V (monoclinic Cc), phase VI (monoclinic Cc) with the transition temperatures 332 K, 302 K, 275 K, 181 K and 101 K respectively.

† E-mail: ista@icmp.lviv.ua.
‡ E-mail: natalie@icmp.lviv.ua.

0953-8984/98/317079+12$19.50

The proton subsystem and the rearrangement of the hydrogen-bond network, in particular, play an important role in the phase transitions, as is supported by the experimental observations [7–9] as well as by the theoretical investigations [10, 11]. At the same time, the results of x-ray diffraction studies, and Raman and NMR spectroscopy measurements [14, 12, 13, 9] indicate the central importance of the XO_4-group angular displacements and the orientational dynamics of these groups in the processes of the proton transport in super-ionic phases, in the low-temperature phase transitions that occur with the formation of the dimer structures of the appropriate geometry and in the crystal deformation that occurs on cooling.

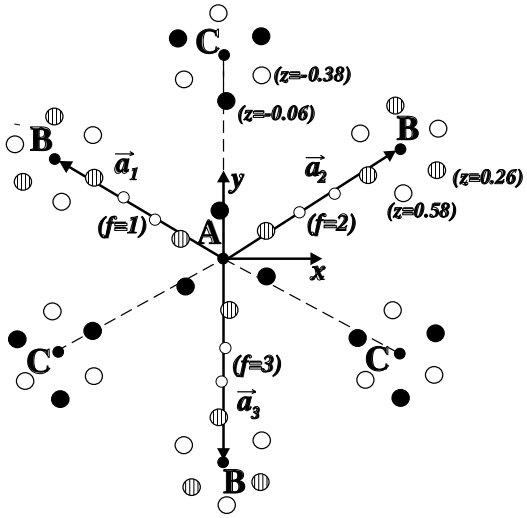

Figure 1. The projection of the rhombohedral primitive cell of TAHSe with the lattice vectors $\boldsymbol{a}_1$, $\boldsymbol{a}_2$, $\boldsymbol{a}_3$ on the (001) plane in the hexagonal setting in phase II. The open, solid and hatched big circles correspond to the possible positions of O(2) oxygens with different values of the fractional height z; A ($z = 0, 0.2$), B ($z = \frac{1}{3}, 0.53$) and C ($z = -\frac{1}{3}, -0.13$) denote the positions of the Se atoms of the lower and upper SeO_4 groups. The small circles indicate the positions of the protons within the hydrogen bond.

In this work, TAHSe is selected for consideration because its complex sequence of phases with two super-ionic (I, II) and two ferroelastic (III, IV) phases of different symmetries among them. The basic crystal structure of TAHSe in the super-ionic phase II in the rhombohedral coordinate system with lattice vectors

$$\boldsymbol{a}_1 = \left(-\frac{\sqrt{3}}{2}a_0,\ \frac{1}{2}a_0,\ \frac{1}{3}c\right) \qquad \boldsymbol{a}_2 = \left(\frac{\sqrt{3}}{2}a_0,\ \frac{1}{2}a_0,\ \frac{1}{3}c\right) \qquad \boldsymbol{a}_3 = \left(0,\ -a_0,\ \frac{1}{3}c\right)$$

(where $a_0 = 3.5$ Å, $c = 22.904$ Å) is shown in figure 1. There are two SeO_4 groups and three virtual hydrogen bonds, $f = 1, 2, 3$ (three possible proton positions), adjacent to the upper SeO_4'' group in the unit cell with lattice vectors $\boldsymbol{R}_m = m_1\boldsymbol{a}_1 + m_2\boldsymbol{a}_2 + m_3\boldsymbol{a}_3$. Another three hydrogen bonds connected with the SeO_4' group belong to the neighbouring unit cells with the vectors $\boldsymbol{R}_m - \boldsymbol{a}_f$. In phase II, the SeO_4 tetrahedra deviate by 4° from the symmetrical positions required by the space group $R\bar{3}m$, whereas in phase I these complexes occupy randomly the two orientationally symmetrical positions with equal probability, which gives rise to the three mirror planes above $T_{\mathrm{II}-\mathrm{I}}$ [7]. The deflections of the vertex oxygens O(2)

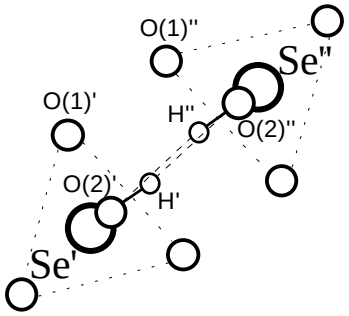

Figure 2. The structure of the hydrogen bond of C_i symmetry in phase II; Se atoms are denoted by big circles, oxygen atoms by medium-sized circles and the equilibrium positions for protons within the bond by small circles.

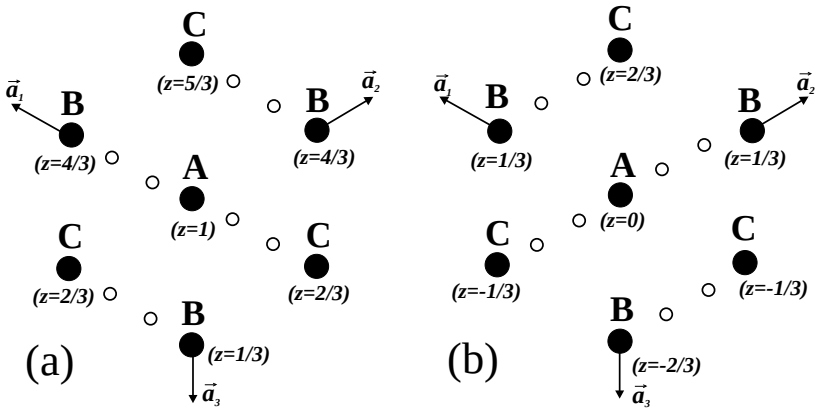

Figure 3. The projection of the hydrogen-bond network structure of TAHSe on the (001) plane in the hexagonal setting in phase III; the hydrogen bonds form sequences along the $\boldsymbol{a}_1$- and $\boldsymbol{a}_2$-directions with the step height $c/3$. Cases (a) and (b) are distinguished by the translation by c along the hexagonal axis; the structural modulation corresponds to the doubling of the lattice period along the $\boldsymbol{a}_3$-direction.

involved in the virtual-hydrogen-bonding formation couple with the proton on the hydrogen bridge and this manifests itself in the H-bond geometry in phase II (figure 2).

The transition into the triclinic phase III is accompanied by a doubling of the primitive unit cell along one of the translation vectors $\boldsymbol{a}_f$ that corresponds to the star $\{\boldsymbol{k}_4\} = \{\frac{1}{2}\boldsymbol{b}_1,\ \frac{1}{2}\boldsymbol{b}_2,\ \frac{1}{2}\boldsymbol{b}_3\}$ in Kovalev notation [15]. The structure of the hydrogen-bonded system for the case of $\boldsymbol{k}_4 = \frac{1}{2}\boldsymbol{b}_3$ is shown in figures 3 and 4. In this case alternating sequences of dimer chains along the $\boldsymbol{a}_1$- (figure 3(a)) and $\boldsymbol{a}_2$- (figure 3(b)) directions are formed. The detailed structure of such dimers consisting of $(SeO_4)'$ and $(SeO_4)''$ groups connected by hydrogen bridges is shown in figure 4. We can see that SeO_4 tetrahedra are reorientated and fixed in one direction that correlates with the forming of the hydrogen bond with C_i symmetry [16].

Unlike the case for phase III, the proton positions with the same index f in the monoclinic phase IV are occupied, which corresponds to the aligning of the dimer chains

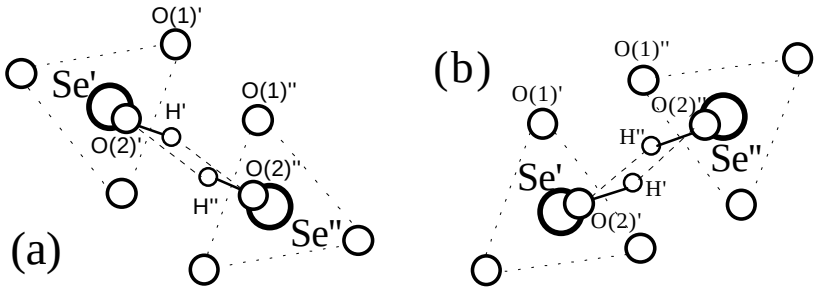

Figure 4. Hydrogen bonds of C_i symmetry along the (a) $\boldsymbol{a}_1$-direction and (b) $\boldsymbol{a}_2$-direction in phase III for TAHSe. The case of the $\boldsymbol{k}_3 = \frac{1}{2}\boldsymbol{b}_3$ orientation state.

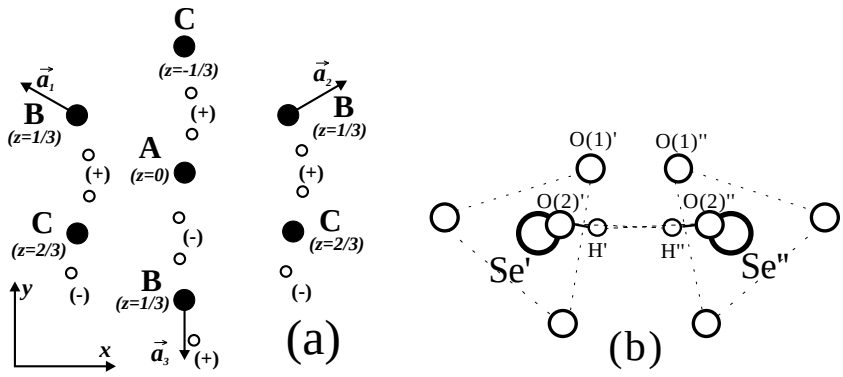

Figure 5. (a) The projection of the hydrogen-bond network structure of TAHSe on the (001) plane in the hexagonal setting in phase IV; the hydrogen bonds $\{+, -, +, \ldots\}$ form sequences along the $\boldsymbol{a}_3$-direction with the step height $c/3$; $x(+) - x(-) = 0.05$. (b) The detailed structure of the C_2-symmetric hydrogen bond in phase IV.

in one direction (figure 5(a)). However, in this phase, $(SeO_4)'$ and $(SeO_4)''$ tetrahedra are reorientated in opposite directions (see figure 5(b)). This results in the alternative shifts of the C_2-symmetric H bonds by $\pm\delta$ ($\delta = 0.025b$ where b is the lattice parameter in phase IV) in the (x, y) plane. The crystalline structure that appears is characterized by the wave vector $\boldsymbol{k}_8 = \frac{1}{2}(\boldsymbol{b}_1 + \boldsymbol{b}_2 + \boldsymbol{b}_3)$.

The rearrangement of the hydrogen-bond network and the role of the proton subsystem in the transformations from phase I to phases III and IV was studied in [17] in the framework of the lattice-gas model. In this case the Hamiltonian has the following form:

$$H = \frac{1}{2}\sum_{\substack{mm'\\ff'}} \Phi_{ff'}(mm')n_{mf}n_{m'f'} - \mu\sum_{mf} n_{mf} \tag{1}$$

where $n_{mf} = \{0, 1\}$ is the proton occupation number for position f in the primitive unit cell at $\boldsymbol{R}_m$; $\Phi_{ff'}(mm')$ is the energy of the proton interactions; μ denotes the chemical potential which determines the average proton concentration. Investigations of the thermodynamic properties of the proton subsystem in the mean-field approximation (MFA) and by using the cluster expansion method have been carried out in [17, 18]. The proposed proton ordering model covers the main features of the transitions from the super-ionic phase to the

ferroelastic phases III and IV of TAHSe and similar compounds, giving an explanation for the principal changes of the proton arrangements. Nevertheless, it was noted that although the consideration of the proton subsystem does provide the possibility of describing the phase transitions I–III or I–IV occurring for example in $Rb_3H(SeO_4)_2$ and $(NH_4)_3H(SO_4)_2$ crystals, it does not allow one to obtain the phase sequence II–III–IV observed in TAHSe. It is essential to study the properties of the proton subsystem together with the surrounding ionic groups in order to understand better the mechanism of the structural ordering in this type of crystal. Therefore, in this work the influence of the SeO_4-tetrahedra reorientations on the proton ordering is considered. In the following analysis it is shown that these interactions lead to crucial changes in the form of the phase diagram in comparison to the case considered previously in [17].

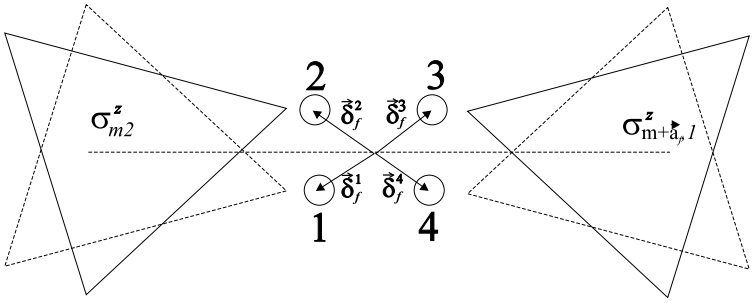

Figure 6. A schematic diagram of the structure of the $(SeO_4)'$–H–$(SeO_4)''$ dimer. The triangles denote two possible orientation states of SeO_4 tetrahedra; the circles identify the positions of the protons within the hydrogen bond.

2. Microscopic description of the proton–ionic group coupling

On the basis of the data from the structural investigations of phases I and II, one is led to assume that ionic groups can be located only at two orientationally symmetric positions relatively to the mirror planes (see figure 6). In this case it is natural to introduce a pseudospin variable for the description of the orientational dynamics of SeO_4 groups. We distinguish two states for each ionic group:

$$\sigma^z_{mk} = \begin{cases} -1/2 & \text{for clockwise rotational displacement} \\ 1/2 & \text{for anticlockwise rotational displacement} \end{cases}$$

where m denotes the index of the primitive unit cell in the crystal and the sublayer index $k = \{1, 2\}$ corresponds to the lower $(SeO_4)'$ group and upper $(SeO_4)''$ group respectively.

The rotations of the neighbouring tetrahedra in one direction are accompanied by the occupation of the positions 1, 3 or 2, 4 by protons with equal probabilities (phases II and III with the C_i symmetry of the hydrogen bond), whereas the opposite rotations of tetrahedra are connected with the occupation of positions 1, 4 or 2, 3 (phase IV with the C_2-symmetric hydrogen bond).

Thus, on this basis, the Hamiltonian (1) for the proton subsystem can be generalized by introducing a set of the possible proton positions $\nu = \{1, 4\}$ between the tetrahedra. This

leads to the dependence of the modulation of the proton interactions

$$\Phi_{ff'}(mm') \to \Phi_{ff'}(mm';\sigma)$$
$$\Phi_{ff'}(mm';\sigma) = \sum_{\nu,\nu'} \Phi_{ff'}^{\nu\nu'}(mm')\left(\frac{1}{2} + (-1)^{\nu}\sigma^z_{m_1,k_1}\right)\left(\frac{1}{2} + (-1)^{\nu'}\sigma^z_{m_2,k_2}\right) \tag{2}$$

on the mutual orientations of the neighbouring tetrahedra. Here the indices attached to the pseudospin variables have the following meanings:

$$(m_1,k_1) = \begin{cases} (m,2) & \nu = 1,2 \\ (m+\boldsymbol{a}_f,1) & \nu = 3,4 \end{cases}$$

$$(m_2,k_2) = \begin{cases} (m',2) & \nu' = 1,2 \\ (m'+\boldsymbol{a}_{f'},1) & \nu' = 3,4. \end{cases}$$

Since the deviations of the proton positions from the centre of the hydrogen bond are small, it is sufficient to expand the interaction $\Phi_{ff'}^{\nu\nu'}(mm')$ into a multipole series in terms of the proton position vectors $\boldsymbol{\delta}_f^{\nu}$, $\boldsymbol{\delta}_{f'}^{\nu'}$ (see figure 6). In this case we have

$$\begin{aligned}\Phi_{ff'}(mm';\sigma) = {} & \Phi_{ff'}^{(0)}(mm') + A_{ff'}^{(f)}(mm')(\sigma^z_{m2} - \sigma^z_{m+\boldsymbol{a}_f,1}) + A_{ff'}^{(f')}(mm')(\sigma^z_{m'+\boldsymbol{a}_{f'},1} - \sigma^z_{m'2}) \\ & + B_{ff'}^{(f)}(mm')(\sigma^z_{m2} + \sigma^z_{m+\boldsymbol{a}_f,1}) + B_{ff'}^{(f')}(mm')(\sigma^z_{m'+\boldsymbol{a}_{f'},1} + \sigma^z_{m'2}) \\ & + C_{ff'}(mm')(\sigma^z_{m+\boldsymbol{a}_f,1} - \sigma^z_{m2})(\sigma^z_{m'+\boldsymbol{a}_{f'},1} - \sigma^z_{m'2})\end{aligned} \tag{3}$$

where

$$\begin{aligned}\Phi_{ff'}^{(0)}(mm') &= \frac{1}{16}\sum_{\nu\nu'}\Phi_{ff'}^{\nu\nu'}(mm') \\ A_{ff'}^{(f)}(mm') &= \frac{1}{2}\sum_{\alpha=\{1,3\}}\nabla_\alpha\Phi(\boldsymbol{R}_{mf} - \boldsymbol{R}_{m'f'})(\delta_f^{2\alpha} - \delta_f^{1\alpha}) \\ B_{ff'}^{(f)}(mm') &= \frac{1}{4}\sum_{\alpha\beta}\nabla_\alpha\nabla_\beta\Phi(\boldsymbol{R}_{mf} - \boldsymbol{R}_{m'f'})(\delta_f^{2\alpha}\delta_f^{2\beta} - \delta_f^{1\alpha}\delta_f^{1\beta}) \\ C_{ff'}^{(f)}(mm') &= -\sum_{\alpha\beta}\nabla_\alpha\nabla_\beta\Phi(\boldsymbol{R}_{mf} - \boldsymbol{R}_{m'f'})(\delta_f^{1\alpha} - \delta_f^{2\alpha})(\delta_{f'}^{1'\beta} - \delta_{f'}^{2'\beta})\end{aligned} \tag{4}$$

with $\boldsymbol{\delta}_f^1 = -\boldsymbol{\delta}_f^3$, $\boldsymbol{\delta}_f^2 = -\boldsymbol{\delta}_f^4$.

The coefficients A, B and C in (4) correspond to the dipole–charge, quadrupole–charge and dipole–dipole interactions respectively. The dipole components are present only for the antiphase reorientations of the neighbouring ionic groups, i.e. the case of phase IV, when $\sigma^z_{m2} = -\sigma^z_{m+\boldsymbol{a}_f,1}$. The resulting dipole moments correspond to the above-mentioned alternating displacements of the hydrogen bonds in phase IV ($\delta = |\boldsymbol{\delta}_2 - \boldsymbol{\delta}_1|$). The quadrupole terms survive for in-phase reorientations ($\sigma^z_{m2} = \sigma^z_{m+\boldsymbol{a}_f,1}$; phases II and III). In particular, for the orientationally ordered state in phase II

$$\begin{aligned}\Phi_{ff'}(mm';\sigma) &= \tilde{\Phi}_{ff'}(mm') \\ \tilde{\Phi}_{ff'}(mm') &= \Phi_{ff'}^{(0)}(mm') + B_{ff'}^{(f)}(mm') + B_{ff'}^{(f')}(mm').\end{aligned} \tag{5}$$

We can describe the orderings with the average pseudospins $\bar{\sigma}^z_{mk}$ playing the role of the order parameters by including in the Hamiltonian, besides (3), terms which distinguish the

differences in energy (w or w') of the hydrogen bonds of C_2 and C_i symmetry:

$$H' = w\sum_{mf}\left\{\left(\frac{1}{2}-\sigma^z_{m1}\right)\left(\frac{1}{2}+\sigma^z_{m-\boldsymbol{a}_f,2}\right)+\left(\frac{1}{2}+\sigma^z_{m1}\right)\left(\frac{1}{2}-\sigma^z_{m-\boldsymbol{a}_f,2}\right)\right\}n_{m-\boldsymbol{a}_f,f}$$
$$+\,w'\sum_{mf}\left\{\left(\frac{1}{2}+\sigma^z_{m1}\right)\left(\frac{1}{2}+\sigma^z_{m-\boldsymbol{a}_f,2}\right)\right.$$
$$\left.+\left(\frac{1}{2}-\sigma^z_{m1}\right)\left(\frac{1}{2}-\sigma^z_{m-\boldsymbol{a}_f,2}\right)\right\}n_{m-\boldsymbol{a}_f,f}$$
$$=\frac{1}{2}(w+w')\sum_{mf}n_{mf}+2(w-w')\sum_{mf}\sigma^z_{m+\boldsymbol{a}_f,1}\sigma^z_{m2}n_{mf}. \tag{6}$$

The short-range interaction between the neighbouring lower and upper sublayers of SeO_4 tetrahedra which belong to the same unit cell and the long-range interaction between these ionic groups in crystal are given by

$$H'' = -K\sum_m \sigma^z_{m1}\sigma^z_{m2}-\frac{1}{2}\sum_{\substack{mm'\\kk'}}J_{kk'}(mm')\sigma^z_{mk}\sigma^z_{m'k'}. \tag{7}$$

The resulting Hamiltonian of the Ising type for pseudospins describes the transition from phase I ($\bar{n}_{mf}=1/3$, $\bar{\sigma}^z_{mk}=0$) to phase II ($\bar{n}_{mf}=1/3$, $\bar{\sigma}^z_{mk}\neq 0$). Despite the fact that the proton subsystem in the super-ionic phase II is disordered, the orientations of the tetrahedra are already frozen in, whereas the vertex oxygens O(2) remain averaged between three possible positions. At the transitions into the orientation state with vector $\boldsymbol{k}_3=\frac{1}{2}\boldsymbol{b}_3$ of phase III or into phase IV, the pseudospin averages can be represented as

$$\bar{\sigma}^z_{mk}=\sigma_0+p_k(m)\exp(\mathrm{i}\boldsymbol{k}_3\cdot\boldsymbol{R}_m)+q_k(m)\exp(\mathrm{i}\boldsymbol{k}_8\cdot\boldsymbol{R}_m). \tag{8}$$

In these phases $\bar{n}_{mf}\neq 1/3$ and $\bar{\sigma}^z_{mk}\neq 0$.

In general, the amplitudes $p_k(m)$ and $q_k(m)$ depend both on the sublattice index in the primitive unit cell and the cell number that relates to the doubling of the translation period with the vectors of the $\{\boldsymbol{k}_4\}$ star in phase III as well as to the structure modulation characterized by vector $\boldsymbol{k}_8$ in phase IV.

Hereafter we shall confine our attention to the consideration of the proton part of the Hamiltonian, taking into account the effect of the pseudospin subsystem in the mean-field-type approximation. In this case, we set the values of $\bar{\sigma}^z_{mk}$ such that they correspond to phase II. The Hamiltonian is thereby returned to the initial type of (1), with the bilinear interaction term $\tilde{\Phi}_{ff'}(mm')$, which possesses the lower symmetry $R\bar{3}$ of phase II rather than that of phase I considered in [17].

3. Proton orderings with the $R\bar{3}$ prototype phase symmetry

The effective lattice-gas Hamiltonian of the type (1), in the MFA, takes the following form:

$$H_{\mathrm{MF}}=U_0+\sum_{mf}(\gamma_f(m)-\mu)n_{mf} \tag{9}$$

where

$$\gamma_f(m)=\sum_{m'f'}\tilde{\Phi}_{ff'}(mm')\bar{n}_{m'f'} \tag{10}$$

are the internal fields, and

$$U_0 = -\frac{1}{2}\sum_{\substack{mm'\\ff'}} \tilde{\Phi}_{ff'}(mm')\bar{n}_{mf}\bar{n}_{m'f'}. \tag{11}$$

The thermodynamic potential of the proton subsystem in this case is given by

$$\Omega = U_0 - \Theta\sum_{mf} \ln(1 + \exp[-\beta(\gamma_f(m) - \mu)]). \tag{12}$$

The average proton occupancies $\bar{n}_{mf}$ can be determined from

$$\bar{n}_{mf} = \frac{\bar{n}}{3} + \delta\bar{n}_{mf}$$

where the deviations $\delta\bar{n}_{mf}$ become nonzero in the phases with proton ordering. For the description of the transition into the ordered phases III and IV, let us expand $\delta\bar{n}_{mf}$ in terms of both the star $\{\boldsymbol{k}_4\}$ vectors and the vector $\boldsymbol{k}_7 = 0$ (here the influence of the surroundings, which results in the H-bond shifts in phase IV, is neglected for simplicity). In particular, for the case of the orientation state characterized by the vector $\boldsymbol{k}_3 = \frac{1}{2}\boldsymbol{b}_3$,

$$\delta\bar{n}_{mf} = \tilde{u}_f \exp(\mathrm{i}\boldsymbol{k}_3 \cdot \boldsymbol{R}_m) + \tilde{v}_f \tag{13}$$

where the deviation amplitudes $\tilde{u}_f$ and $\tilde{v}_f$ can be found from the conditions for the minimum of the free energy $F = \Omega + \mu\bar{n}N$ for the given average proton concentration $\bar{n}$ ($\bar{n} = 1$ for $M_3H(XO_4)_2$-type crystals):

$$\frac{\partial F}{\partial \bar{n}_{m'f'}} = 0 \tag{14}$$

or from the system of equations which follows immediately from (14):

$$\bar{n}_{mf} = \left\{1 + \exp[\beta(\gamma_f(m) - \mu)]\right\}^{-1}. \tag{15}$$

In the case of $R\bar{3}$ symmetry, the Fourier transform of the interaction matrix $\tilde{\Phi}_{ff'}(\boldsymbol{k})$ has the following form for $\boldsymbol{k} = \boldsymbol{k}_3$:

$$\begin{aligned}
&\tilde{\Phi}_{11}(\boldsymbol{k}_3) = \varphi_1 + \xi \qquad \tilde{\Phi}_{22}(\boldsymbol{k}_3) = \varphi_1 - \xi \qquad \tilde{\Phi}_{33}(\boldsymbol{k}_3) = \varphi_3\\
&\tilde{\Phi}_{12}(\boldsymbol{k}_3) = \tilde{\Phi}_{21}(\boldsymbol{k}_3) = \varphi_2 \qquad \tilde{\Phi}_{13}(\boldsymbol{k}_3) = \tilde{\Phi}_{31}(\boldsymbol{k}_3) = \varphi_4 + \eta\\
&\tilde{\Phi}_{23}(\boldsymbol{k}_3) = \tilde{\Phi}_{32}(\boldsymbol{k}_3) = \varphi_4 - \eta
\end{aligned} \tag{16}$$

where ξ and η are the deviations connected with the disappearance of the mirror planes in phase II. For the case of the $R\bar{3}m$ symmetry of the prototype phase I, $\xi = \eta = 0$.

We can build up the linear combinations of $\tilde{u}_f$ and $\tilde{v}_f$ which play the role of the order parameters. For this purpose, we expand $\tilde{u}_f$ and $\tilde{v}_f$ in terms of the eigenvectors of the Fourier transform matrices $\tilde{\Phi}_{ff'}(\boldsymbol{k}_3)$ and $\tilde{\Phi}_{ff'}(\boldsymbol{k} = 0)$ respectively, and furthermore retain the terms related to the maximum eigenvalues of these matrices (in this way the components corresponding to the maximum temperature of the transition into the ordered state are taken into consideration). The resulting form for $\delta\bar{n}_{mf}$ is given by

$$\begin{aligned}
\delta\bar{n}_{m1} &= \frac{1}{\sqrt{2}}(1 + \delta_2)u\exp(\mathrm{i}\boldsymbol{k}_3 \cdot \boldsymbol{R}_m) + \frac{1}{\sqrt{6}}v\\
\delta\bar{n}_{m2} &= -\frac{1}{\sqrt{2}}(1 - \delta_2)u\exp(\mathrm{i}\boldsymbol{k}_3 \cdot \boldsymbol{R}_m) + \frac{1}{\sqrt{6}}v\\
\delta\bar{n}_{m3} &= \delta_3 u\exp(\mathrm{i}\boldsymbol{k}_3 \cdot \boldsymbol{R}_m) - \frac{2}{\sqrt{6}}v.
\end{aligned} \tag{17}$$

Here

$$\delta_2 = \frac{\varphi_4\eta - (\varphi_2 + \varphi_3 - \varphi_1)\xi/2}{\varphi_2(\varphi_2 + \varphi_3 - \varphi_1) - \varphi_4^2} \qquad \delta_3 = \frac{1}{\sqrt{2}}\frac{\varphi_4\xi - 2\varphi_2\eta}{\varphi_2(\varphi_2 + \varphi_3 - \varphi_1) - \varphi_4^2}.$$

Setting $\xi = \eta = 0$, the representations $\delta\bar{n}_{mf}$ [17] for the case of the prototype phase with the higher symmetry $R\bar{3}m$ can be deduced. With this constraint, $\bar{n}_1^+ = \bar{n}_2^-$ and $\bar{n}_1^- = \bar{n}_2^+$ (the labels $\{+, -\}$ correspond to even and odd indices m_3 in the mth unit cell respectively). We emphasize that, unlike in the latter case, the average proton occupancies $\bar{n}_1^+$ and $\bar{n}_2^-$ as well as $\bar{n}_1^-$ and $\bar{n}_2^+$ are now different.

Substitution of (17) into (10) and (11) yields

$$\gamma_1(m) = \gamma_0 + av + (b + \Delta_b)\exp(\mathrm{i}\boldsymbol{k}_3 \cdot \boldsymbol{R}_m)u$$
$$\gamma_2(m) = \gamma_0 + av - (b - \Delta_b)\exp(\mathrm{i}\boldsymbol{k}_3 \cdot \boldsymbol{R}_m)u$$
$$\gamma_3(m) = \gamma_0 - 2av + b_3\exp(\mathrm{i}\boldsymbol{k}_3 \cdot \boldsymbol{R}_m)u$$

$$U_0 = -\frac{N}{2}\gamma_0 - \frac{N}{2}\sqrt{6}av^2 - \frac{N}{2}\sqrt{2}(b + b_1)u^2$$

where

$$a = \frac{1}{\sqrt{6}}[\tilde{\Phi}_{11}(0) - \tilde{\Phi}_{12}(0)] \qquad b = \frac{1}{\sqrt{2}}[\varphi_1 - \varphi_2 + \delta_2\xi + \sqrt{2}\delta_3\eta]$$

$$\Delta_b = \frac{1}{\sqrt{2}}[\xi + \delta_2(\varphi_1 + \varphi_2) + \sqrt{2}\delta_3\varphi_4] \qquad b_3 = \frac{1}{\sqrt{2}}[2\eta + 2\delta_2\varphi_4 + \sqrt{2}\delta_3\varphi_3]$$

$$b_1 = \delta_2\Delta_b + \frac{1}{\sqrt{2}}\delta_3 b_3 \qquad \gamma_0 = \frac{1}{3}\bar{n}\sum_{f'}\tilde{\Phi}_{ff'}(0).$$

The order parameters u and v should be determined from the conditions for the minimum of the free energy:

$$\frac{\partial}{\partial u}\left(\frac{1}{N}F\right) = 0 \qquad \frac{\partial}{\partial v}\left(\frac{1}{N}F\right) = 0 \tag{18}$$

together with the solution of the equation for the chemical potential μ:

$$\frac{\partial}{\partial \mu}\left(\frac{1}{N}F\right) = 0. \tag{19}$$

The transition into the ordered state corresponding to phase III occurs for $u \neq 0$ and $v \neq 0$ (with $\bar{n}_1^+ \to 1$, $\bar{n}_2^+ \to 0$, $\bar{n}_3^+ \to 0$ or $\bar{n}_1^- \to 0$, $\bar{n}_2^- \to 1$, $\bar{n}_3^- \to 0$ when $|u| \to b/[\sqrt{2}(b + b_1)]$ and $v \to 1/\sqrt{6}$). The solutions $u = 0$ and $v \neq 0$ are related to the case of phase IV ($\bar{n}_3^+ = \bar{n}_3^- \to 1$; $\bar{n}_1^+$, $\bar{n}_1^-$, $\bar{n}_2^+$, $\bar{n}_2^- \to 0$ for $v \to -2/\sqrt{6}$).

Numerically solving the system of equations (18), (19) and selecting the solutions which determine the absolute minimum gives different sequences of phase transitions according to the value of the ratio $\tilde{b} = b/a$. The temperature dependences of the order parameters for different values of $\tilde{b}$ are plotted in figure 7. In particular, for $\tilde{b} < \tilde{b}^*$, where $\tilde{b}^* \simeq 1.6$ is the triple point, the first-order transformation II–IV occurs. It should be noted that, for a sufficiently narrow interval with $\tilde{b} > \tilde{b}^*$, the region of existence of the two-phase-transition sequence II–III–IV appears; in this case the III–IV transformation is of first order. With further increase of $\tilde{b}$, the temperature interval for which the phase IV exists narrows until only the transition II–III remains, which is first order for $\tilde{b} < \tilde{b}_c$ and second order for $\tilde{b} > \tilde{b}_c$ where $\tilde{b}_c$ is the tricritical point. The resulting $(\tau, \tilde{b})$ phase diagram (where $\tau = kT/|a|$) is represented in figure 8. We can see that, in contrast to the case with $\xi = \eta = 0$ studied in [17], for which the III–IV coexistence line was parallel to the temperature axis, in the

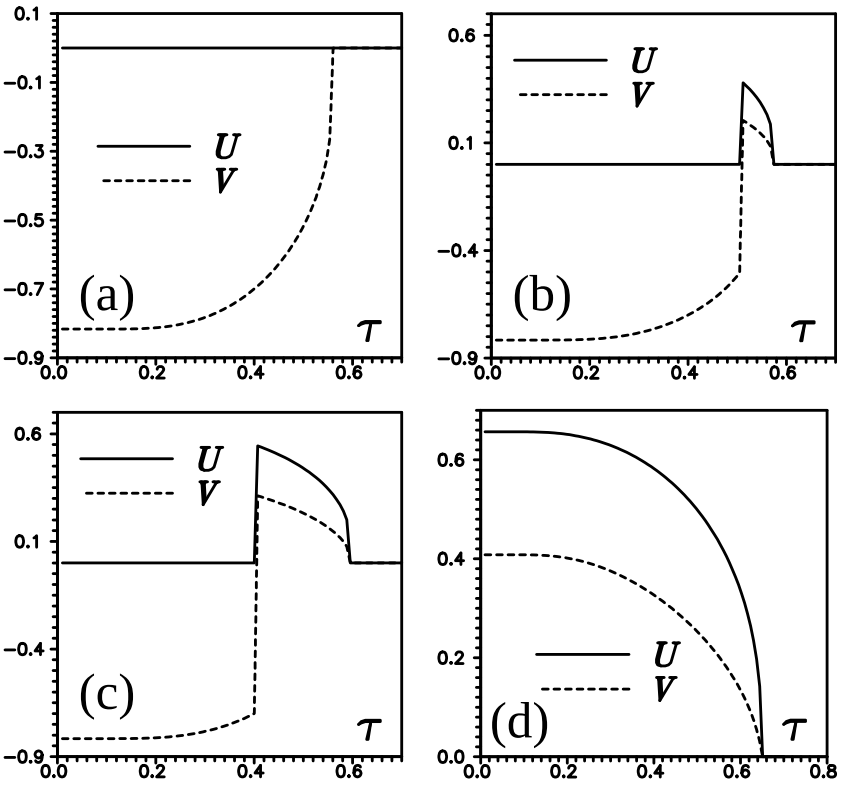

Figure 7. The dependence of the order parameters on τ for $\Delta_b/|a| = 0.6$, $b_3/|a| = -0.6$, $b_1/|a| = -0.15$ and (a) $\tilde{b} = 1.55$, (b) $\tilde{b} = 1.65$, (c) $\tilde{b} = 1.75$, (d) $\tilde{b} = 1.95$.

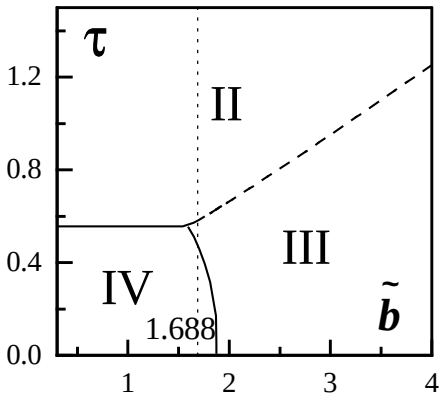

Figure 8. The $(\tau, \tilde{b})$ phase diagram for $\Delta_b/|a| = 0.6$, $b_3/|a| = -0.6$, $b_1/|a| = -0.15$; the full and broken curves indicate the first- and second-order phase transitions respectively. The dotted line corresponds to the value $\tilde{b} = 1.688$ obtained for TAHSe.

diagram obtained, this coexistence curve is bent towards the right. This effect leads to the appearance of the III–IV phase transformation in TAHSe on cooling that was observed in experiments.

Using the Ewald technique for the lattice series summation to obtain the Coulomb contribution to the proton interaction potential, we can evaluate, from the available structural data, the values of the parameters a and b. Taking the inter-proton distance to be the separation between the centres of the hydrogen bonds in phase II for TAHSe, we obtain $a = -0.09$ eV, $b = -0.15$ eV and $b/a = \tilde{b}_0 = 1.688$, which is very close to the triple point $\tilde{b} = \tilde{b}^*$ and falls in the range $\tilde{b}^* < \tilde{b} < \tilde{b}_c$. In other words, the phase sequence II–III–IV is obtained for TAHSe on cooling with both transitions first order. This agrees with the experimentally observed situation for this crystal.

Moreover, it is clear that the values b and a connected with the Fourier transform components of the proton interaction matrix change with the hydrostatic pressure P that is applied. This occurs due to the changes of the lattice parameters under deformation. The dependence $\tilde{b} = \tilde{b}(P)$ has been calculated by the Ewald method, and the results obtained and the (T, P) phase diagrams were discussed comprehensively in [19]. We merely note that the temperature at which the super-ionic transition occurs decreases with pressure, and the steep slope of the III–IV transition temperature induced by the pressure increase agrees with the diagram obtained by Gesi [20].

4. Conclusions

We have performed studies of the influence of SeO_4-tetrahedra reorientations on the proton subsystem with the aim of elucidating the mechanism of the structural ordering occurring in $M_3H(XO_4)_2$-type super-ionic crystals. In particular, it follows from our results that the orientational ordering of SeO_4 ions which takes place at a considerably higher temperatures than is required for the proton orderings is deeply involved in the I $\rightarrow$ II $\rightarrow$ III $\rightarrow$ IV phase transitions and appears to be the principal mechanism determining the observed phase sequence in TAHSe.

However, we did not carry out self-consistent investigations of the properties of the pseudospin subsystem together with the proton orderings. In fact, the average pseudospin values $\bar{\sigma}^z_{mk}$ for phase IV were set to the values for phase II; hence we did not obtain the ordering of tetrahedra occurring in this phase. Further work is needed on this, as well as on the effect of the deformations in the crystal appearing on cooling, which can change the energies of the C_2- and C_i-symmetric hydrogen bonds.

Nevertheless, the resulting phase diagrams obtained with the values of the parameters calculated for TAHSe agree with the experimental data for the phase orderings. With the constraint $\xi = \eta = 0$, I–III and I–IV transitions occur, which correspond to the cases of $Rb_3H(SeO_4)_2$ and $(NH_4)_3H(SO_4)_2$ crystals with only one super-ionic phase of $R\bar{3}m$ symmetry. The pressure dependence of the transition temperature obtained for these crystals as well as that for TAHSe are consistent with the experimental measurements [20, 21], which confirms our main assumptions concerning the nature of the microscopic processes occurring in $M_3H(XO_4)_2$.

References

[1] Bohn A, Melzer R, Sountag R, Lechner R E, Schuck G and Langer K 1995 *Solid State Ion.* **77** 111
[2] Melzer R, Wessels T and Reehnis M 1996 *Solid State Ion.* **92** 119
[3] Komukae M, Sakata K, Osaka T and Makita Y 1994 *J. Phys. Soc. Japan* **63** 1009
[4] Merinov B V, Bolotina N B, Baranov A I and Shuvalov L A 1988 *Crystallografiya* **33** 1387
[5] Pietraszko A, Lukaszewicz K and Augustyniak M A 1992 *Acta Crystallogr.* C **48** 2069
[6] Pietraszko A and Lukaszewicz K 1993 *Bull. Polish Acad. Sci.* **41** 157
[7] Lukaszewicz K, Pietraszko A and Augustyniak M A 1993 *Acta Crystallogr.* C **49** 430

[8] Merinov B V, Antipin M Yu, Baranov A I, Tregubchenko A M, Shuvalov L A and Struchko Yu T 1991 *Crystallografiya* **36** 872
[9] Belushkin A V, Carlile C J and Shuvalov L A 1995 *Ferroelectrics* **167** 21
[10] Salejda W and Dzhavadov N A 1990 *Phys. Status Solidi* b **158** 119
[11] Salejda W and Dzhavadov N A 1990 *Phys. Status Solidi* b **158** 475
[12] Abramič D, Dolinšek J, Blinc R and Shuvalov L A 1990 *Phys. Rev.* B **42** 442
[13] Raimbault G, Romain F and Lautie A 1992 *J. Raman Spectrosc.* **23** 147
[14] Kamoun M, Halouani M and Daoud A 1987 *Phase Transitions* **9** 327
[15] Kovalev O B 1986 *Irreducible and Inductive Representations and Corepresentations of Fedorov Groups* (Moscow: Nauka) (in Russian)
Kovalev O B 1965 *Irreducible Representations of the Space Groups* (New York: Gordon and Breach)
[16] Katrusiak A 1993 *Phys. Rev.* B **48** 2992
[17] Stasyuk I V, Pavlenko N and Hilczer B 1997 *Phase Transitions* **62** 135
[18] Stasyuk I V, Pavlenko N and Hilczer B 1998 *J. Korean Phys. Soc.* **32** S24
[19] Stasyuk I V and Pavlenko N 1997 *Proc. Adriatico Research Conf.: Simple Systems at High Pressures and Temperatures: Theory and Experiment (Trieste, 1997)* (Trieste: ICTP) (ICTP Science Abstract No 54, http://www.ictp.trieste.it/~pub_off/sci-abs/smr999)
[20] Gesi K 1977 *J. Phys. Soc. Japan* **43** 1949
[21] Sinitsyn V V, Baranov A I, Ponyatovsky E G and Shuvalov L A 1995 *Solid State Ion.* **77** 118